

# **Internal Government Studies**

**1995**

## **Reports and Presentations**

**Study Name:**            **Interferometer Thermal  
Sounder [ITS] - Part II**

**Team Members:**       **NOAA/ORA(Mitch Goldberg) &  
NASA/GSFC(Joel Susskind)**

**IPO POC:**               **D. Blersch**

# INTERNAL GOVERNMENT STUDIES - FY 1995

## Interferometer Thermal Sounder [ITS] - Part II

<u>Presentation/Paper Title</u>	<u>Author(s)</u>	<u>Date</u>
"Final Report to the Integrated Program Office on the Interferometer Thermal Sounder Study: Part II"	Susskind, McMillan, Goldberg	15 NOV 95
"IGS Final Presentations for FY95: Interferometer Thermal Sounder (ITS)-[PART II: ITS versus AIRS Tradeoff]"	Goldberg, McMillan, Susskind, Smith, Huang	29 SEPT 95
"IGS Final Presentations for FY95: Interferometer Thermal Sounder (ITS)-Comparative Study of Performance of ITS versus AIRS"	Goldberg, McMillan, Susskind, Smith, Huang	29 SEPT 95
"Interferometer Thermal [Sounder (ITS)-Part II ITS versus AIRS Tradeoff] - Midterm Presentations"	Goldberg, McMillan, Susskind, Smith, Huang	29 JUNE 95
"Primary Differences Between AIRS and ITS"	Joel Susskind	29 JUNE 95
"POES CARD Input for ITS-part II"	Mitch Goldberg	18 APRIL 95
"High Resolution Transmittance for ITS versus AIRS"	Larry McMillan	3 JULY 95
"Preliminary Report on ITS Simulation Study"	Joel Susskind	18 APRIL 95
"ICS Monthly Status Report on ITS"	Mitch Goldberg	18 APRIL 95

National Aeronautics and  
Space Administration  
**Goddard Space Flight Center**  
Greenbelt, MD 20771

g: Hange  
Weit  
B/ers. H



CF San

Reply to Attn of: 910.4

Stan Schneider  
NPOESS, IPO  
Centre Building, Room 1450  
8455 Colesville Rd.  
Silver Spring, MD 20910

Dear Stan:

Enclosed are 5 copies of our final report for Interferometer Thermal  
Sounder: Part II. This shows what has been accomplished thus far  
and also shows that we have laid the groundwork to successfully  
complete the study in FY96, as outlined in our new proposal.

Sincerely,

Joel Susskind  
Laboratory for Atmospheres

Enclosure: 5

**Final Report to the Integrated Program Office**

**on the**

**Interferometer Thermal Sounder Study: Part II**

November 15, 1995

Joel Susskind, NASA/GSFC

Mitch Goldberg, NOAA/ORA

Larry McMillin, NOAA/ORA

## **1. Introduction**

The purpose of this study is to assess the relative performance of the proposed Interferometer Thermal Sounder (ITS) instrument relative to that of the Atmospheric Infra-Red Sounder (AIRS) in

1. its ability to determine atmospheric temperature and moisture profiles, and
2. its ability to meet the IORD threshold sounding requirements.

The methodology to be used is to perform detailed simulations of observations for AIRS and ITS, used in conjunction with AMSU-A and MHS, under a variety of clear and partially cloudy atmospheric and surface conditions. These observations are then analyzed using state-of-the-art methodologies to determine and assess the accuracy of the corresponding atmospheric temperature and moisture profiles.

The simulations are performed using our best estimate of the instruments' response to the geophysical parameters of the scene with the addition of appropriate noise characteristics. Given the simulated observations, retrievals are done separately by two groups: the NOAA group consisting of Larry McMillin and Mitch Goldberg, using the NOAA retrieval algorithm; and the NASA group, Joel Susskind and Chris Barnet, using the NASA retrieval algorithm.

All participants are members of, or associated with, the AIRS Science Team and the retrieval algorithms used are those developed by these groups for their use in analysis of AIRS/AMSU/MHS data. The detailed simulation methodology developed by the AIRS Science Team is used in this study. In order for the comparison test to be fair, the same simulation methodology, including radiative transfer assumptions and approximations, has to be used to assess both AIRS and ITS. For this reason, we had to create an appropriate monochromatic line-by-line transmittance calculation data base for use in simulating both AIRS and ITS observations.

Given the instrumental characteristics, instrument observations can be simulated as a function of scene in a straightforward manner. We can generate high resolution (0.01

$\text{cm}^{-1}$  ) radiance for a specific atmosphere (i.e., temperature, humidity, ozone profiles, and clouds) from 500 to 3000  $\text{cm}^{-1}$  . A high resolution interferogram is constructed from a cosine transform of the simulated photons absorbed by the detector as a function of mirror position. The interferogram can be truncated, apodized, and sub-sampled to produce a simulated interferogram for a specific instrument. The detector, instrument, and "scene" noise can be simulated directly, as well as effects due to motion of the spacecraft during sampling of the interferogram. The methodology, using a monochromatic line-by-line data base, is not computationally practical, however, because of the need to store and use tables for roughly 250,000 frequencies in the spectral domain sampled by the instruments. For this reason, it is a common practice to use tables of channel transmittances, derived from the monochromatic line-by-line data base via rapid transmittance algorithms. These algorithms work well for the non-negative and localized channel response of AIRS. Channel response functions, similar to those of AIRS, can be obtained for an interferometer if appropriate apodization functions are applied in the analysis of interferometer data. Construction of rapid transmittance algorithms for apodized interferometer spectra is, therefore, not a problem. The disadvantage of apodization is a potential loss in spectral resolving power. On the other hand, if the spectra to be analyzed are unapodized, as proposed by the proponents of ITS, the problem becomes more complicated as the channel response functions are no longer localized in the spectral domain.

The need to simulate and analyze unapodized interferometric data posed a difficult problem for our study. In addition, we needed reasonable noise estimates to be used in the simulation of ITS observations. The noise estimates, calculated by Lincoln Laboratories, produced an unexpected result, in that the instrumental noise was shown to be a function of the characteristics of the Earth scene being observed. This further complicated the problem in that we needed to develop methodology to compute appropriate ITS noise characteristics as a function of geophysical parameters in the scene and, furthermore, account for the variable noise in the retrieval process. For these reasons, the study could

not be completed in FY95.

Because of complications resulting from non-localized channel response functions, as well as scene dependent noise, we have chosen to break the problem into three segments. Our initial studies have indicated that noise and band coverage issues can be addressed separately. The loss of spectral information due to coverage and sampling differences of ITS as compared to AIRS, as well as preliminary estimates of differences in signal-to-noise, are addressed in this report. Hamming apodized ITS channel response functions can be used to easily extend this study and provide insight into the effect of the loss of resolution of ITS compared to AIRS caused by apodization. We can then suggest a minimum optical path difference for an apodized interferometer which would be needed to achieve the sounding goals. These experiments would also take into account the proper scene dependence of the noise in the apodized ITS spectra.

The "real" test, however, will be to simulate the performance of the unapodized instrument in a full retrieval with realistic profiles and cloudy conditions. No algorithm currently exists for simulating observations or performing retrievals of this accuracy, complexity, and throughput using unapodized channel response functions. We did not anticipate the complexity of the problem. We have been successful in simulating unapodized observations of an interferometer using Fourier transforms of monochromatic radiances. This method would be prohibitive, however, even for our limited study and its implications for operational sounding would be extremely negative. We have embarked on a path that has yielded a *novel and effective new approach*, which may well be a breakthrough in processing unapodized interferograms. With our method we can still utilize a rapid algorithm for absorption coefficients and can handle the negative and non-localized side lobes of the effective channel response functions of an unapodized interferometer.

As of Oct. 31, 1995 we have:

- Reported preliminary results of retrieval performance implications of ITS considering only the effects of ITS channel noise and band coverage, but using AIRS channel

response functions (June 2, 1995);

- Reported results of an apodization study and reported a proposed plan of action to complete the study (Sept. 29, 1995);
- Added interferometer experts to our team to assist in instrument simulations and noise estimates;
- Estimated effects of non-localized channel response functions on radiances and developed an algorithm which will enable utilization of a rapid algorithm in the unapodized case;
- Created rapid-algorithm coefficients for the Hamming apodized ITS case.

These advances lay the groundwork for completing a comprehensive study of ITS versus AIRS in FY96. Each of the items above will be discussed below in detail.

Other issues must be addressed at some point for an interferometer proposed for an advanced sounder, that are beyond the scope of this study. Some of the issues still open for a long life-cycle advanced interferometric sounder are:

- Motion compensation. Motion compensation appears to be a critical requirement for an interferometer, such as ITS, because of the instrument's sensitivity to variations in the total scene flux. With our ability to simulated the interferometer this effect will be easy to study, if necessary.
- Non-contiguous field of views (FOV's). A controversial issue is to what extent small non-spatially contiguous FOV's improve the probability of detecting clear regions and, if so, is the trade-off of non-contiguous FOV's worth the increase in probability.
- The need for detector redundancy. The AIRS has two detectors at each sample location ( $781.2 \leq \nu \leq -2673.8 \text{ cm}^{-1}$ ) and samples twice per resolution element.
- Risk assessment of new design features, such as the porch swing mechanism and the low emissivity beam-splitter.

## 2. Preliminary noise and coverage simulations

The first simulations we performed were done to begin to assess the effects of differences in spectral sampling and signal to noise of ITS versus AIRS.

The AIRS instrument has a full-width-at-half-maximum (FWHM) of  $\Delta\nu \approx \nu/1200$  in all channels and is sampled twice per “resolution” element (*i.e.*,  $\approx \nu/2400$ ). The spectrum is divided into 17 bands, in which linear detector arrays are used to sample 2378 unique frequencies. The spectral characteristics of the AIRS instrument are given in table 1. The first 15 bands utilize bi-linear arrays and, therefore, have 2 detectors per array.

**Table 1: AIRS specifications (Aumann and Pagano 1994)**

band	grating order	wavenumber coverage ( $\text{cm}^{-1}$ )	resolution (FWHM) ( $\text{cm}^{-1}$ )	sampling interval ( $\text{cm}^{-1}$ )	# samp	# det	det. type
1	11	2551.0-2673.8	2.1	1.05	118	236	PV
2	10	2433.1-2557.5	2.1	1.07	116	232	PV
3	10	2309.5-2433.1	1.9	0.95	130	260	PV
4	9	2169.2-2309.5	1.9	0.96	150	300	PV
5	6	1540.8-1612.9	1.4	0.71	105	210	PV
6	6	1459.9-1526.7	1.3	0.64	105	210	PV
7	6	1336.9-1440.9	1.1	0.55	192	384	PV
8	5	1283.7-1338.7	1.2	0.59	100	200	PV
9	5	1216.5-1272.3	1.1	0.53	100	200	PV
10	4	1054.9-1135.1	1.0	0.51	159	318	PV
11	4	972.8-1044.9	0.9	0.44	167	334	PV
12	4	909.9- 972.8	0.75	0.38	167	334	PV
13	4	851.1- 903.3	0.66	0.33	161	322	PV
14	3	788.0- 851.8	0.76	0.38	167	334	PV
15	3	727.3- 781.2	0.65	0.33	167	334	PV
16	3	687.3- 727.8	0.57	0.28	144	144	PC
17	3	649.4- 681.7	0.50	0.25	130	130	PC

The NOAA and GSFC retrieval algorithms use carefully selected subsets of critical channels within each band to improve algorithm performance and execution speed. The remainder

of the channels are still necessary for AIRS because:

- Instrumental shifts in frequency *or* detector outages may require a different sub-set of channels to maintain the selection of critical channels over the 7 year lifespan of AIRS.
- Instrument calibration requires additional channels.
- Retrievals of trace species require some additional channels, not considered in the NASA and NOAA critical list.

Moreover, the bi-linear arrays and integrated read out circuits provide the total channel set at virtually no additional cost.

The ITS instrument has 3 bands, where each band has a constant spectral sampling interval and spectral resolution. The sampling of an interferometer is a function of the maximum path difference,  $L$ , and the optical filter which defines the band window. Since an interferometer's signal to noise,  $S/N$ , is dependent on the total flux incident on the detector, the designers of ITS made the windows narrower. We used the most recent estimates of the selected spectral domains and associated noise figures from Lincoln Laboratories study (Kerekes, 1995b). The "resolution" of an interferometer, given by the FWHM, is dependent on the choice of apodization used. For an unapodized interferometer, the FWHM is roughly equal to the spectral sampling interval. Apodization does not affect the sampling interval, but broadens the effective resolution.

The ITS spectral specifications are summarized in Table 2. Typically, authors quote the unapodized resolution as  $1/2L$ . This is not accurate and in Table 2 we have defined the FWHM of the central lobe as the resolution, which is equal to  $1.2/2L$ . The ITS band coverage, sampling, and unapodized resolution is illustrated in figure 1. The AIRS resolution is exactly twice the sampling and is a function of wavenumber, while the ITS resolution and sampling is constant for each band.

**Table 2: ITS specifications (Kerekes, 1995a)**

band	L (cm)	coverage ( $\text{cm}^{-1}$ )	FWHM (apodized)	FWHM (unapodized)	N	sampling ( $\text{cm}^{-1}$ )
1	0.8	620-1095	1.14	0.754	760	0.64
2	0.4	1210-1540	2.27	1.508	264	1.26
3	0.2	2155-2450	4.54	3.017	118	2.56

Lincoln Laboratories provided to us the channel noise estimates of ITS for four cases:

- HM = Hot ( $\approx 300$  K) troposphere and moderate stratosphere ( $\approx 260$  K).
- MH = Moderate troposphere ( $\approx 270$  K) and hot stratosphere ( $\approx 300$  K)
- CC = Cold troposphere ( $\approx 230$  K) and cold stratosphere ( $\approx 240$  K).
- 250 = a constant temperature of 250 K

Amongst the four cases HM generally has the largest noise and CC the lowest. Figure 2 shows the spectral channel irradiance noise estimate,  $NE\Delta N$ , for AIRS, ITS CC, and ITS HM. Also shown are the specifications to which AIRS was designed. These specifications were based on simulations showing noise values required to meet the sounding requirements of  $1^\circ$  RMS errors in 1 km layers in the troposphere. Figure 3 shows the noise estimates reported as  $NE\Delta T$  at a 250 K brightness temperature. ITS noise is generally larger than that of AIRS, especially at the shorter wavelengths, and is larger than the specification at some frequencies.

Three runs were conducted using the NASA algorithm and summarized in table 3. In all three cases the retrieval algorithm and forward calculation is identical, but the channel selection and noise values differ. All runs used a subset of AIRS channels. The first run is a typical channel set used for analysis of AIRS data. The columns labeled "ITS" do not use channels outside of the ITS spectral domain nor do they include AIRS channels that are sampled more often than the ITS sampling specification. Four temperature sounding channels, not typically used to analyze AIRS data, were added in the  $650 \leq \nu \leq 750$   $\text{cm}^{-1}$  region to improve the ITS results.

**Table 3: Number of Channels Used in Study**

retrieval	AIRS	ITS CC	ITS HM
temperature	149	81	81
surface	64	37	37
water	66	44	44
ozone	31	15	15
cloud	29	21	21

In figure 4 we show the spectral coverage of the two instruments and channels selected for use in the AIRS retrievals done at GSFC. The dark solid lines at the top of the chart show the spectral regions *not* measured by AIRS. The bracketed lines show spectral regions covered by ITS. We would expect the ITS surface retrieval to suffer, since 19 channels in the  $2450 \leq \nu \leq 2675 \text{ cm}^{-1}$  region are not measured by ITS. We would expect this to affect the accuracy of the retrieved value of surface solar reflectance,  $\rho$ , since these channels provide the most information about  $\rho$ . In addition, their loss may result in degradation in the accuracy of other retrieved surface parameters (*e.g.*,  $T_s$ , spectral emissivity). Seven channels are also lost in the  $1095 \leq \nu \leq 1210 \text{ cm}^{-1}$  window region, which probably contain redundant information and should have little effect.

The ITS water retrieval should be affected by loss of many channels in all three gap regions, but primarily at the short wavelength end during the daytime. The loss of many of the weak lines near  $2600 \text{ cm}^{-1}$  will affect the retrieval near the surface during the day and the loss of channels in the  $1540\text{-}1600 \text{ cm}^{-1}$  region may affect the retrieval in the upper troposphere.

A set of 100 “Phillips” profiles was used, which is the standard set for the AIRS simulation runs (Susskind *et al.*, 1995). We took one of the best cases from the AIRS simulations: daytime conditions with 50% cloudiness at 300 mb. The ITS HM and CC noise estimates, summarized in figures 2 and 3, were used for all 100 scenes in the two ITS runs, and the AIRS noise estimate was used for the AIRS runs. All runs assumed

the instruments were accompanied by an AMSU-A and MHS, using appropriate noise estimates. The cloud clearing methodology for a single cloud layer case requires use of two adjacent spots or fields of view (FOV) to correct for cloud effects. We also used simulated data for two MHS 15 km spots and one AMSU-A 50 km spot. Stratospheric sounding channels do not see clouds, effectively reducing the channel noise by  $\sqrt{2}$  because observations in both spots can be averaged together.

Figure 5 shows RMS errors of the retrieved temperature profile for

- o AIRS/AMSU-A channels with predicted AIRS noise,
- o AIRS/AMSU-A channels with ITS sampling and CC noise,
- o AIRS/AMSU-A channels with ITS sampling and HM noise, and
- o AMSU-A channels alone.

Values shown are RMS errors in 1 km layer mean temperatures from the surface to 200 mb, 2 km layer mean temperatures from 200 mb to 100 mb, and 4 km layer mean temperatures from 100 mb to 1 mb. The tropospheric RMS error (average RMS error in layers from the surface to 200 mb) and the average RMS error over all layers, are indicated in the caption. These results are summarized in table 4, which also include the surface skin temperature error. The main factor affecting the difference in these results is the channel noise. Temperature sounding channels in the  $15\mu m$  region, with frequencies from  $650\text{ cm}^{-1}$  to  $750\text{ cm}^{-1}$ , affect the results primarily above 300 mb, while channels in the  $4.2\mu m$  region,  $2200\text{ cm}^{-1}$  to  $2400\text{ cm}^{-1}$ , affect results primarily beneath 300 mb. Consequently, based on noise considerations alone, AIRS would perform slightly poorer in the stratosphere because ITS noise is predicted to be better in the  $15\mu m$  region. Conversely, AIRS would perform better in the lowest 2 km when ITS CC noise is used and throughout the troposphere when ITS HM noise is used. The surface skin temperature error, as shown in table 4, degrade significantly when ITS HM noise is used.

**Table 4: Results of Simulation, RMS errors in °C**

instrument	scene	T(P=200-1000)	T(P=1-1000)	T <sub>surf</sub>	q <sub>total</sub>
AMSU	n/a	1.62	1.57	–	20.77
AIRS	n/a	1.00	1.11	0.36	1.38
ITS	HM	1.11	1.14	0.62	10.85
ITS	CC	1.01	1.07	0.41	8.92

Figure 6 shows RMS errors, in percent, of layer precipitable water in 1 km layers from the surface to 200 mb for the same four cases. The caption of the figure includes the RMS errors of the total column precipitable water in both % and g/cm<sup>2</sup>. The statistic used is equivalent to percent errors in specific humidity, and is a more stringent and appropriate test than percent errors in relative humidity. For example, if the true relative humidity in a layer is 20%, and the retrieval is 30%, the percent error in layer precipitable water would be 50%, rather than a 10% error in relative humidity.

Most information about the water vapor profile above the boundary layer comes from the spectral region between 1300 cm<sup>-1</sup> and 1600 cm<sup>-1</sup>. In this region, all noise levels are better than the specifications and are relatively close to each other, though HM noise increases rapidly near 1500 cm<sup>-1</sup>, which is sensitive to upper tropospheric water vapor. AIRS noise and sampling performs better than ITS at the highest tropospheric levels as a result of combination of increased spectral domain (see figure 4) and lower noise. The biggest improvement using AIRS noise and sampling compared to ITS noise and sampling is in the critical boundary layer below 700 mb. This is a result primarily of the ability to use channels at frequencies greater than 2500 cm<sup>-1</sup> which are highly sensitive to boundary layer water vapor during the day. Note that percent errors in the lowest 2 km are almost a factor of two smaller when AIRS noise and sampling are used, compared to ITS noise and sampling. Furthermore, total precipitable water is measured more accurately by more than a factor of five by AIRS.

This initial study is extremely preliminary and addresses only part of the problem. The purpose of this study was to give an order of magnitude estimate of the problem. In reality, the results can be quite misleading because

- a) the AIRS channel locations and channel response functions were used instead of the ITS apodized or unapodized channel response functions with appropriate channel sampling,
- b) ITS noise was not computed as a function of scene, but was used as a constant for all cases,
- c) The cloud characteristics in the case we chose was one of the most stable cloud cases in our simulations. Many other cases are more sensitive to effects of instrumental noise in the  $4\ \mu m$  region.

The next sets of retrievals to be performed must address these problems. Further research is needed to appropriately handle the considerations in both (a) and (b). We have done considerable work to prepare to use the appropriate ITS channel response functions. This is detailed below. First we discuss the problem of using an apodized response functions. Then we show research we have done to allow for the case of unapodized channel response functions.

### 3. Study of apodization functions

The channel response function for an unapodized interferometer is given by a  $\sin(x)/x$  function and is shown as a dotted line in figure 7. The  $\sin(x)/x$  function is non-localized and has large negative side-lobes. Apodization is a filtering process that effectively adds channels together in such a way as to minimize the effects of the side-lobes. The result can be a localized channel response function with a loss in resolution, as illustrated by the Hamming apodization function in figure 7.

We investigated many forms of apodization functions to ensure that we would not de-

grade the effective spectral resolution of the instrument beyond necessary limits. Apodization functions can be represented by a “tradeoff” curve, as shown in figure 8. The unapodized  $\sin(x)/x$  function has the best resolution, defined as full width at half maximum (FWHM), which we will normalize and call “FWHM=1”. The  $\sin(x)/x$  function has large side-lobes, the first two are -22% and +13% of the central lobe. In fact, only 33% of the area of the response function falls within  $\pm \text{FWHM}/2$  (one  $\Delta\nu$ ) for the unapodized case, and 41% within  $\pm \text{FWHM}$  (two  $\Delta\nu$ ). The equivalent numbers for AIRS are 72% and 95%. This shows a large loss in spectral purity for the unapodized case. Apodization causes a decrease in the percentage of side-lobes at the expense of spectral resolution, as shown in figure 8, giving the percent of the height of the two side-lobes compared to that of the central lobe. Results of a number of different apodization functions are shown. We can “tune” the apodization to any desired side-lobe level but the corresponding FWHM cannot be better than the values shown in this figure. We chose the Hamming apodization function because

- The side-lobes are approximately 1% of the central lobe.
- The FWHM is *only* 50% larger than the  $\sin(x)/x$  function.
- It is a well published and well understood function.

Another method of illustrating the “tradeoff” between localized and non-localized behavior of the channel response functions is to calculate the percentage of the signal within the central lobe of the function. This is shown as a function of FWHM for a set of apodization functions in figure 9. Again, the Hamming function (shown diamond in figure) is at the “knee” of the tradeoff curve where 86% of the signal is within the central lobe versus only 37% contained in the central lobe of the  $\sin(x)/x$  function. The Kaiser-Bessel function ( $k=5$ ) has an advantage that its side-lobes “fall off” more rapidly than the Hamming function and, therefore, has more signal contained in the central lobe. The first few side-lobes are larger than those of the Hamming function, however (see figure 8). Therefore, we feel the Hamming is the best apodization function for this study.

The channel response function for a Hamming apodized ITS instrument is also included in figure 7. The spectral shape is very similar to that of AIRS, but its half width is seriously degraded as compared to AIRS for the ITS instrument with  $L=0.8$  cm. In order to get a feeling of the effect of the loss of spectral resolution compared to AIRS, we applied this channel response function and the AIRS channel response function to a high-resolution monochromatic simulated Earth spectrum. The results are shown in figure 10 in the temperature sounding  $15\mu m$   $CO_2$  region. The AIRS resolution was specified to resolve the lines of this spectral region to meet the advanced sounding goals. The degradation caused by an effective resolving power of 900 for apodized ITS instead of 1200 for AIRS is seen in this figure. The Hamming apodized ITS does not adequately resolve this region and the temperature soundings can be significantly degraded, primarily in the upper troposphere and stratosphere sounded by this spectral region.

We feel that this exercise justifies calculating the rapid-algorithm coefficients for the Hamming apodization function and performing a set of simulated retrievals to show the degradation of retrieval accuracy with an apodized instrument. In the first simulation, with  $L=0.8$ , the signal to noise, calculated by Lincoln Laboratories, will be used, corrected for the improved characteristics of the Hamming filter (we estimate that  $NE\Delta T$  will be reduced by 20% due to the Hamming filter as compared to that of unapodized spectra)

The rapid algorithm coefficients have been recently calculated for the Hamming apodized ITS channels with  $L=0.8$  cm based on a set of representative profiles by the method of calculating rapid algorithm coefficients used in the AIRS simulation studies (Susskind *et al.*, 1995). After validation of these coefficients, we will begin our retrieval study to correctly simulate the performance of a Hamming apodized ITS instrument. Initially, we propose to use the spectral band coverage indicated in Kerekes (1995a) and noise calculations based on Kerekes (1995b). We will extend our study by using our own noise calculations for a modified ITS by potentially increasing  $L$  and the spectral domain of the bands. Both would help spectral resolution, but degrade the channel noise. Based on these

calculations, we will make recommendations for the minimum value of maximum interferometric optical path difference,  $L$ , needed to meet sounding goals if the interferograms are apodized.

#### 4. Study of non – localized behavior of unapodized interferograms

The effective spectral resolution needed to produce accurate soundings may already be in the ITS instrument, without the need to increase  $L$ , if an unapodized response function is used. The use of unapodized spectra must be tested in the simulation mode, however.

In order to estimate the effects of a non-localized channel response  $\sin(x)/x$  function and also to begin to quantify the extent to which radiances in unapodized spectra are perturbed by response outside of the central lobe, we conducted the following calculation. A high resolution monochromatic simulated Earth radiance spectrum was convolved with a  $\sin(x)/x$  function and compared to the same radiance spectrum convolved with only the central lobe of the  $\sin(x)/x$  function. These two calculations in brightness temperatures are shown in figure 11. The difference between them is shown in the lower panel. The  $\sin(x)/x$  function spectrum (heavy line) produced a spectrum that is very similar to the AIRS simulated spectrum shown in figure 10; however, the amplitude of the variations are considerably larger than that of AIRS (compare to figure 9). One might interpret this as due to ITS having a better spectral resolution as compared to AIRS channel response functions. This is not the case, however. The calculation with only the central lobe does not show this “enhanced” structure.

The difference between these two curves is due to the effects of the  $\sin(x)/x$  side-lobes which can be up to  $\pm 10^\circ$  in this critical temperature sounding region, with RMS differences on the order of  $4^\circ$ . Other regions have even larger effects, up to  $30^\circ$ . These values of contamination are quite high, in our experience, and illustrate that the potential problem of incorporating an unapodized interferometer into our algorithms is much greater than

anticipated earlier. For accurate results, the effects of the side-lobes have to be accounted for to better than the instrumental noise levels.

All retrieval algorithms depend on reasonable estimates of the noise co-variance matrix. In numerical algorithms, the sensitivity of the brightness temperature,  $\Theta$ , of a channel  $i$  to changes in parameter  $X$  (*e.g.*, temperature) is approximated by a finite difference of the forward calculation

$$S_i = \Theta_i(X + \delta X) - \Theta_i(X)$$

while the noise is found by considering the uncertainty in computed brightness temperature due to errors in the estimates of all the other parameters  $Y$  (*e.g.*, water, ozone, surface temperature, etc.) The noise co-variance contains many derivatives of the form

$$N_{ij} = (\Theta_i(X, Y + \delta Y) - \Theta_i(X, Y)) \cdot (\Theta_j(X, Y + \delta Y) - \Theta_j(X, Y))$$

The contamination in non-localized channels can be significantly greater than in a localized channel because, for example, water contamination due to a given line at a given frequency will cause computational noise in **all** channels. In the NASA retrieval algorithm we do not use channels that have obvious contamination by absorption from unwanted species.

Our algorithm optimizes the noise co-variance calculation by selecting a subset of channels with high sensitivity and low computational noise (literally the signal to noise of the sounding parameter) for use in the retrieval process. In order to best account for side-lobes, causing contributions from other channels, most of the interferometer channels are probably needed in the retrieval process to maximize the information content. This could significantly impact the computational power needed to process the data in real time.

## 5. Algorithm development : Simulation of unapodized interferograms

Before we could address the effects of side-lobe contamination on retrieval accuracy we had to address the ability to accurately simulate the unapodized spectra in a reasonable way. The rapid algorithm method for construction of channel transmittances and radiances for localized spectra may not be accurate enough when used for unapodized spectra.

In our early estimates of execution speed, based on monochromatic spectra, we estimated that an accurate fast Fourier transform algorithm would increase our program's execution time by a factor of 1000 or more. This would make it impractical to perform the needed simulation experiments. We therefore felt that we needed an approach where we could utilize the form of our existing rapid algorithm for this study. In this way, we would not only perform a reasonably efficient calculation for our study but we might make some headway into the ability of operational processing for an unapodized interferometer as well.

If we imagine that the  $\sin(x)/x$  function, where  $x$  is proportional to the frequency difference from the center of the channel, can be broken into segments representing separate sub-channels, then we can imagine calculating rapid algorithm coefficients and radiances for each sub-channel, followed by adding the calculated individual radiances together to do the forward calculation for the entire channel. Large numbers of side-lobe rapid algorithm coefficients for each channel would be still be impractical, so we propose the following set of functions.

We will assume that each of the outer side-lobes of the  $\sin(x)/x$  function can be approximated with a symmetric sine function and multiplied by an effective value given by the average value of  $x$  in the side-lobe,  $\bar{x}$ . The first negative and first positive side lobes do not satisfy this symmetry so they must be calculated exactly, as must be the central lobe. We can treat the problem accurately by considering three functions for each channel.

The first function is a combination of the central lobe and the first positive side lobes on either side of the central lobe. The second function is the pair of first negative side

lobes. This function is treated separately from the first function to ensure that effective absorption coefficients for each function are positive. The third function is the symmetric sine function. Mathematically these functions are given by

$$F_1(x) = \frac{\sin(x)}{x} \Big|_{|x| \leq \pi} + \frac{\sin(x)}{x} \Big|_{2\pi \leq |x| \leq 3\pi}, \quad \text{zero elsewhere}$$

$$F_2(x) = \frac{1}{a_1} \cdot \frac{\sin(x)}{x} \Big|_{\pi \leq |x| \leq 2\pi}, \quad \text{zero elsewhere}$$

where  $a_1$  is the height of the first side-lobe and is equal to -0.2172.

$$F_3(x) = \sin(\pi x), \quad |x| \leq 1, \quad \text{zero elsewhere}$$

The  $\sin(x)/x$  function can then be approximated as

$$\frac{\sin(x)}{x} \simeq F_1(x) + a_1 \cdot F_2(x) + \sum_{j=3}^N a_j \cdot [F_3(x - x_j) + F_3(x + x_j)]$$

$j$	$x_j$	$a_j \approx x_j^{-1}$	
1	$2\pi \cdot 0.75$	-0.2172	included in $F_2$
2	$2\pi \cdot 1.25$	+0.1284	included in $F_2$
3	$2\pi \cdot 1.75$	-0.0913	
4	$2\pi \cdot 2.25$	+0.0709	
5	$2\pi \cdot 2.75$	-0.0580	
6	...	...	

These three functions are illustrated in the top three panels of figure 12. The fourth panel shows the combination of a set of functions. The bottom panel shows the difference between this approximation and a  $\sin(x)/x$  function. Each of the three functions is a non-negative localized function and an appropriate rapid transmittance calculation and radiance calculation can easily be done.

The forward radiance for channel  $i$  can then be calculated directly, by combining 2 radiance calculations,  $R_1$  and  $R_2$ , specifically done for the channel of interest, plus a

weighted sum of radiance calculations,  $R_3(k)$ , done for each of the other channels.

$$R(i) \approx R_1(i) + a_1 \cdot R_2(i) + \sum_{j=3}^N a_j \cdot [R_3(i-j) + R_3(i+j)]$$

This form requires three sets of rapid algorithm coefficients and three radiance computations for each channel rather than one, as is now done. Radiance calculations must now be done for all channels, whether we intend to use them in the retrieval process or not, so as to allow for their contribution to the side-lobes of the channels used.

We convolved this approximation for the channel response function with the high resolution monochromatic radiance and compared the result to that obtained with the  $\sin(x)/x$  function applied to the same radiance. This approximation has an RMS error of  $0.055^\circ$  for the  $15\mu m$  band and never exceeds the  $NE\Delta T$  of the instrument ( $0.2^\circ$ ) as shown in figure 13. If the approximation needs to be improved, additional side-lobes can be added to the calculation of  $F_1$  and  $F_2$  until the desired accuracy is achieved, provided the functions remain reasonably localized.

With the progress in approximating the  $\sin(x)/x$  function and selection of an appropriate apodization function we are ready to simulate the ITS instrument with the Lincoln Laboratories estimates for noise. We are also working with our GSFC interferometer experts and Lincoln Laboratories to provide an independent verification of the Lincoln Laboratory noise estimates for the purpose of (i) embedding a scene dependent noise calculation into our algorithm and (ii) extending our study with a modified ITS instrument, if necessary. Therefore, we have successfully solved the open issues, identified as items (a) through (c) on page 12, and have begun implementation of these considerations into the AIRS simulated retrieval algorithms used for the AIRS Science Team evaluations.

## 6. Future Work

A new proposal has been submitted which will address the concerns presented in this final report. The following milestones were addressed in this proposal:

- Jan. 31, 1996. Simulate the instrument noise characteristics for ITS apodized and unapodized cases.

Simulate apodized and unapodized spectra for an ensemble of cases.

Generate rapid algorithm coefficients for apodized ITS and AIRS transmittance functions.

- Mar. 30, 1996. Perform physical retrievals (NASA, NOAA separately) for clear and cloudy apodized spectra and AIRS spectra.

Perform regression retrievals (NOAA) for unapodized spectra.

- June 30, 1996. Develop computationally efficient rapid algorithm for use with unapodized spectra.
- Sep. 30, 1996. Perform and evaluate clear and cloudy retrievals for unapodized spectra (NASA and NOAA). Write final report.

## References :

- Aumann, H.H. and R.J. Pagano 1994. Atmospheric infrared sounder on Earth observing system. Optical Engineering v.33 p.776-784.
- Jimenez, H.J. (1995) Tilt Profile and Modulation Efficiency, Report presented at Camp Springs by Lincoln Labs. (Apr. 20, 1995).
- Joiner, J., J. Susskind and C.D. Barnet 1995. Determination of atmospheric and surface parameters from simulated AIRS/AMSU sounding data. II. Cloud clearing methodology. submitted to J. Atmos. Oceanic Tech.
- Kerekes, John (1995a) Application of ITS spectral regions. presented at Camp Springs by Lincoln Labs. (Apr. 20, 1995).
- Kerekes, John (1995b) written report of ITS  $NE\Delta N$  from scene radiance, Lincoln Labs (June 16, 1995).
- Susskind, J., J. Joiner and C.D. Barnet 1995. Determination of atmospheric and surface parameters from simulated AIRS/AMSU sounding data. I. Retrieval methodology. submitted to J. Atmos. Oceanic Tech.
- 2nd Intn'l Workshop on Atmospheric Science from Space using FTIR (JPL) "Interferometer Thermal Sounder" UW, Hughes, Bomem (Sep. 11, 1991)
- Project Report NOAA-1, "POES High Resolution sounder study: Final Report" Lincoln Labs. and NOAA (Jan. 25, 1993)
- Project Report NOAA-7, "POES Advanced Sounder Study (Phase II). Lincoln Labs. and NOAA (Mar. 17, 1994)

## Figure captions

- 1 Comparison of AIRS and ITS resolution (FWHM) and sampling. The ITS FWHM is given by  $1.2/(2 \cdot L)$  where  $L$  is the maximum optical displacement while the sampling is  $1/(2L)$ . For Hamming apodization the FWHM is given by  $1.8/2L$ .
- 2  $NE\Delta N$  for ITS simulations (Kerekes, 1995b) and the AIRS instrument (Aumann and Pagano, 1994). The dotted curve is the EOS PM-1 specification for  $NE\Delta T$  at 250 K converted to  $NE\Delta N$ . HM is the Lincoln Laboratories hot-troposphere, cold-stratosphere noise estimate. CC is the Lincoln Laboratories cold-troposphere, cold-stratosphere noise estimate.
- 3  $NE\Delta T$  at 250 K for the noise estimates shown in Figure 1.
- 4 Example of a simulated Earth brightness temperature spectrum as seen by AIRS response function. The thick lines at the top of the figure are regions where AIRS does not sample. Also, shown are the three spectral domains where the ITS instrument can make measurements. The \*'s indicate the channels which are used in the NASA AIRS retrievals.
- 5 RMS layer mean temperature errors for the AIRS and ITS simulations. See text for explanation.
- 6 RMS layer mean specific humidity errors for the AIRS and ITS simulations. See text for explanation.
- 7 Channel response functions for AIRS, unapodized ITS, Hamming apodized ITS in the  $15\mu m$  band.
- 8 Tradeoff curve of height of side-lobes versus FWHM for a variety of apodization curves. All FWHM's are normalized to the  $\sin(x)/x$  function. Note that the Hamming apodization function (diamond) is a reasonable tradeoff between small side-lobes and resolution.
- 9 Tradeoff curve of area of central lobe versus FWHM for a variety of apodization curves. All FWHM's are normalized to the  $\sin(x)/x$  function. See text for discussion.

- 10 Illustration of the degradation of resolving power of a Hamming Apodized ITS interferometer in the  $15\mu m$  band. The thin line is a convolution of the AIRS channel response function with a high resolution simulated spectrum at the AIRS sampling interval,  $(\Delta\nu = \nu/1200)$ . The AIRS can resolve the individual lines within the  $CO_2$  vibrational-rotational band. The thick line is the convolution of the ITS  $L = 8$  Hamming apodized channel response function with the same high resolution spectrum at the ITS sampling interval,  $\Delta\nu = (1/2L)$ . The difference between these two curves is shown in the lower panel (differences only taken at ITS sample points).
- 11 Illustration of the effect of the ITS  $\sin(x)/x$  channel response function side-lobes in the  $15\mu m$  band. The thick line shows the convolution of the  $\sin(x)/x$  function with a high resolution simulated spectrum. The thin line is the convolution of only the central lobe of the same  $\sin(x)/x$  function with the same high resolution spectrum. The lower panel shows the difference between these two curves and represents the contribution of the side-lobes.
- 12 Illustration of an approximation method for the  $\sin(x)/x$  function. The function  $F_1$  is a combination of the central lobe and the first pair of positive side lobes. The function  $F_2$  is the first pair of negative side lobes normalized by their height. The function  $F_3$  is a normalized sine function used to represent the remaining lobes of the  $\sin(x)/x$  function. The  $\sin(x)/x$  function is shown in the fourth panel and the difference between the approximation and the  $\sin(x)/x$  function is shown in the fifth panel. Note: if more accuracy is desired additional lobes can be added to  $F_1$  and  $F_2$ .
- 13 Errors in brightness temperature due to the  $\sin(x)/x$  approximation in the  $15\mu m$  band. The thick and thin lines are so close as to not be distinguished in the upper panel.

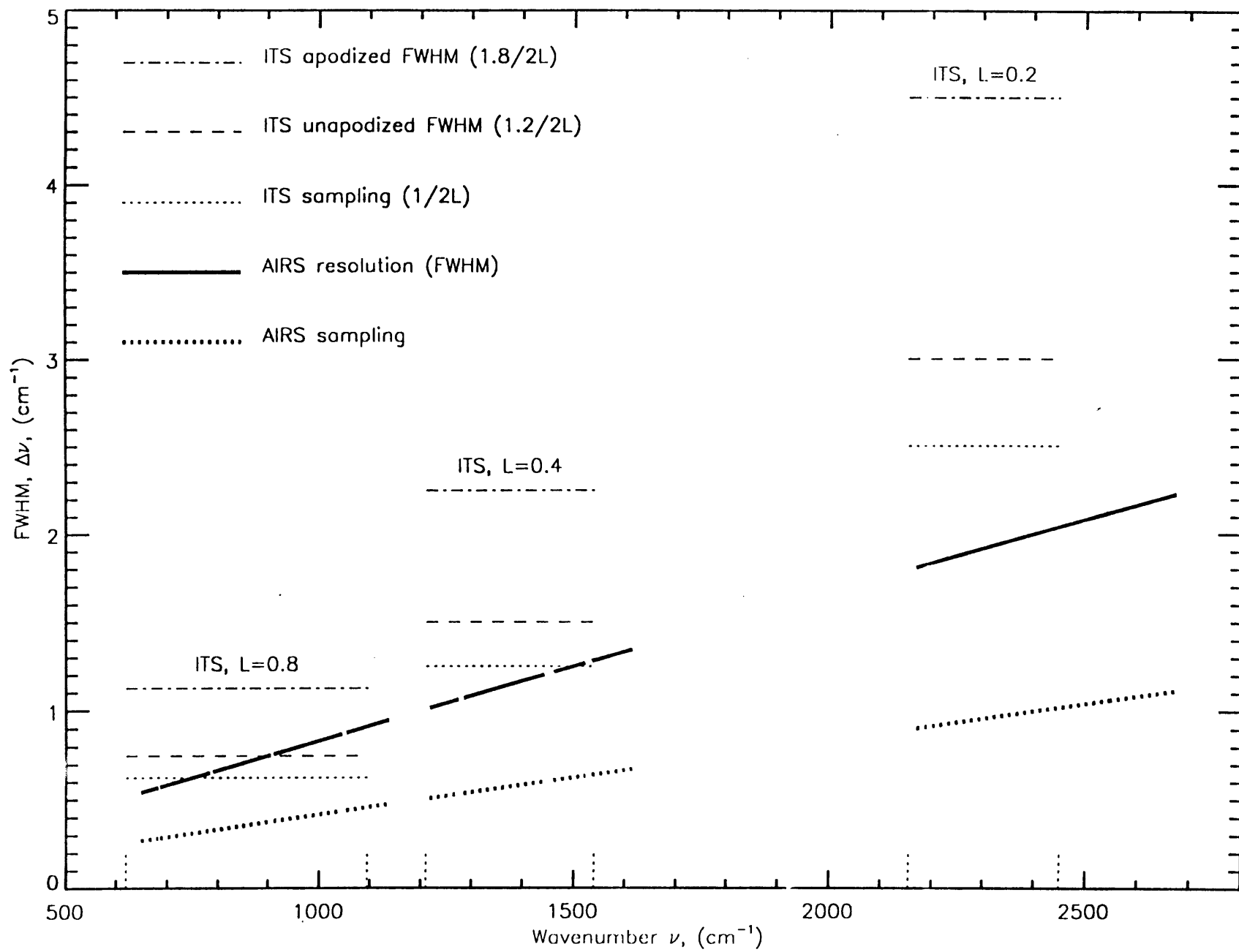


Figure 1

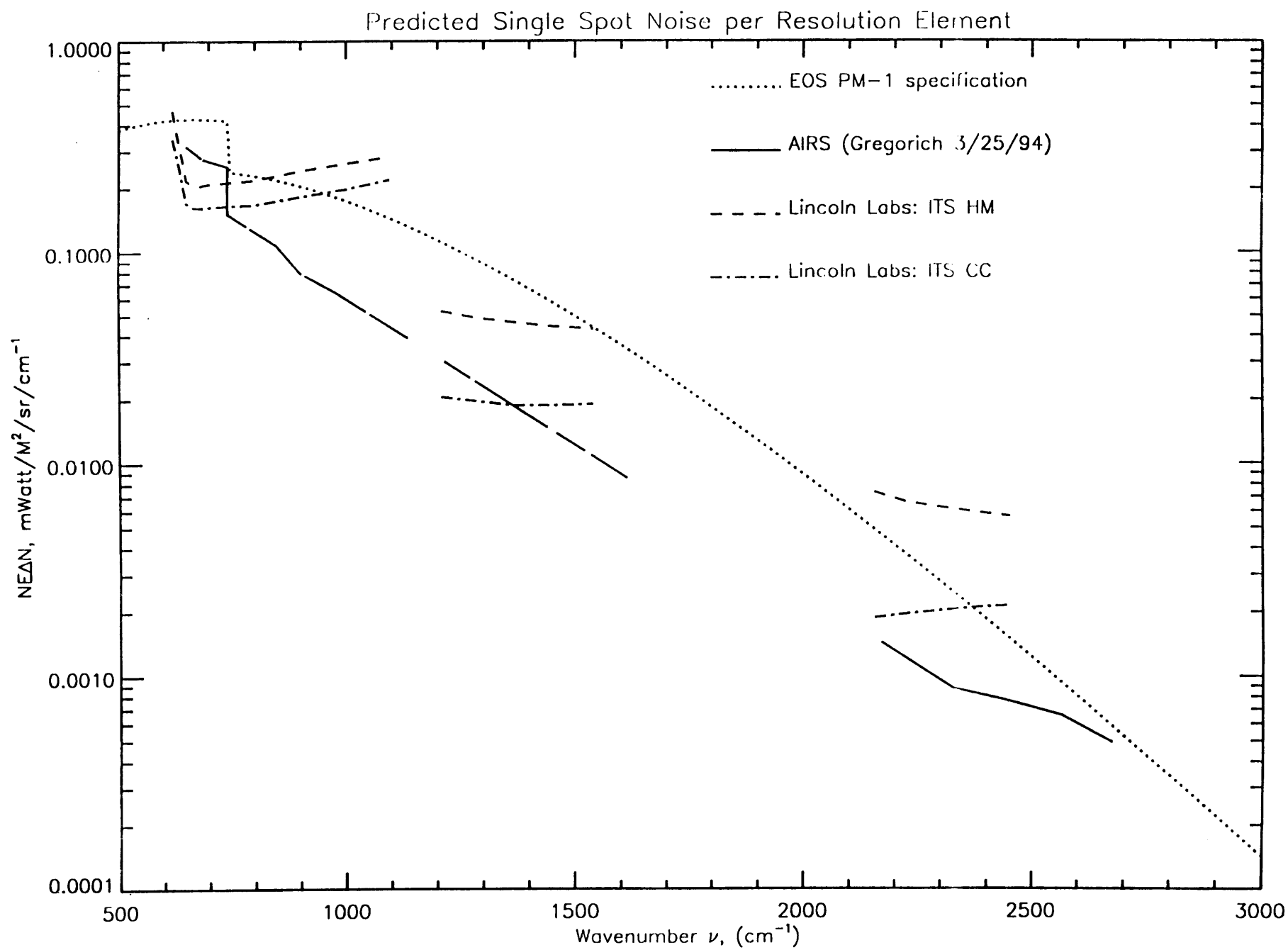


Figure 2

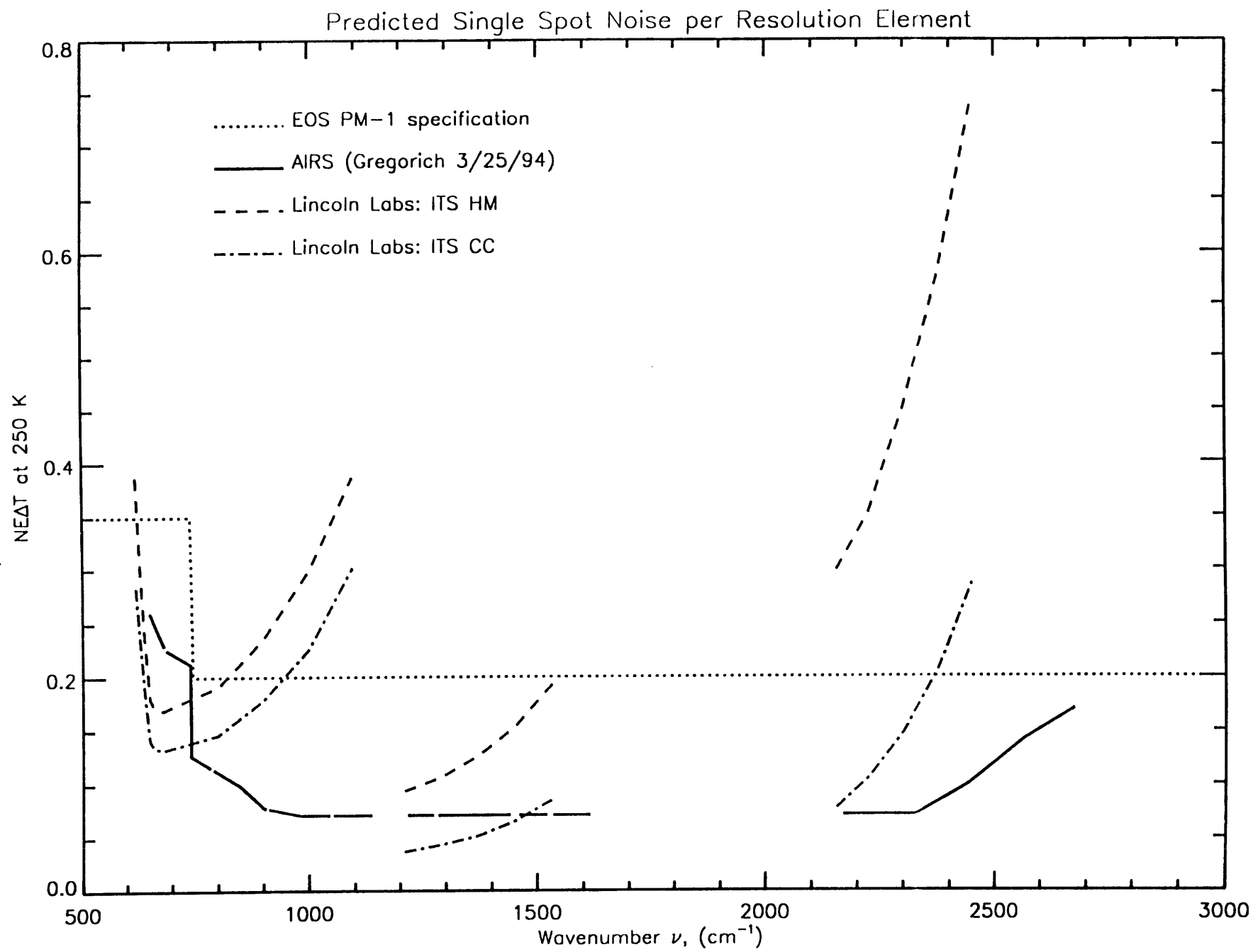


Figure 3

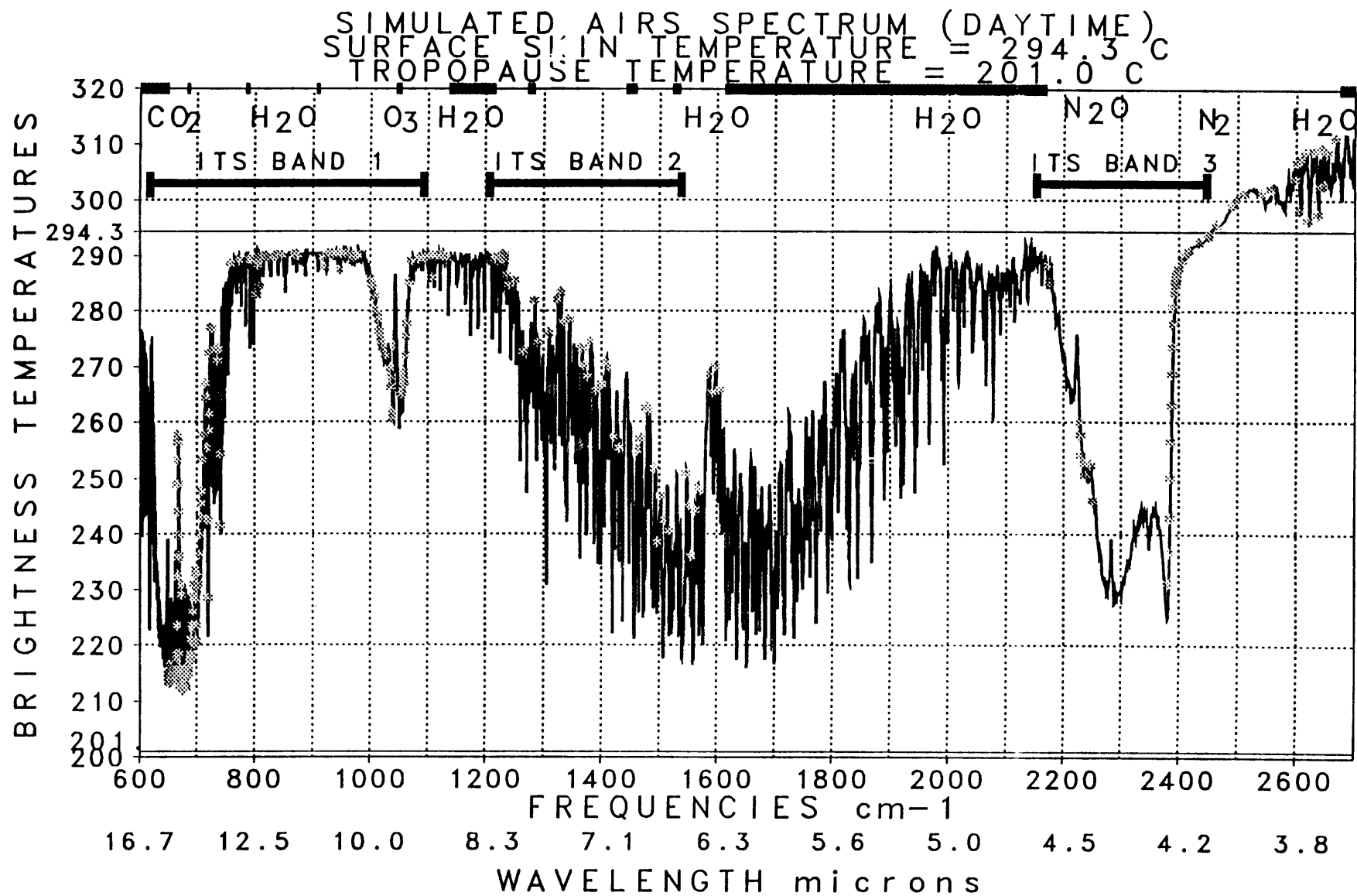
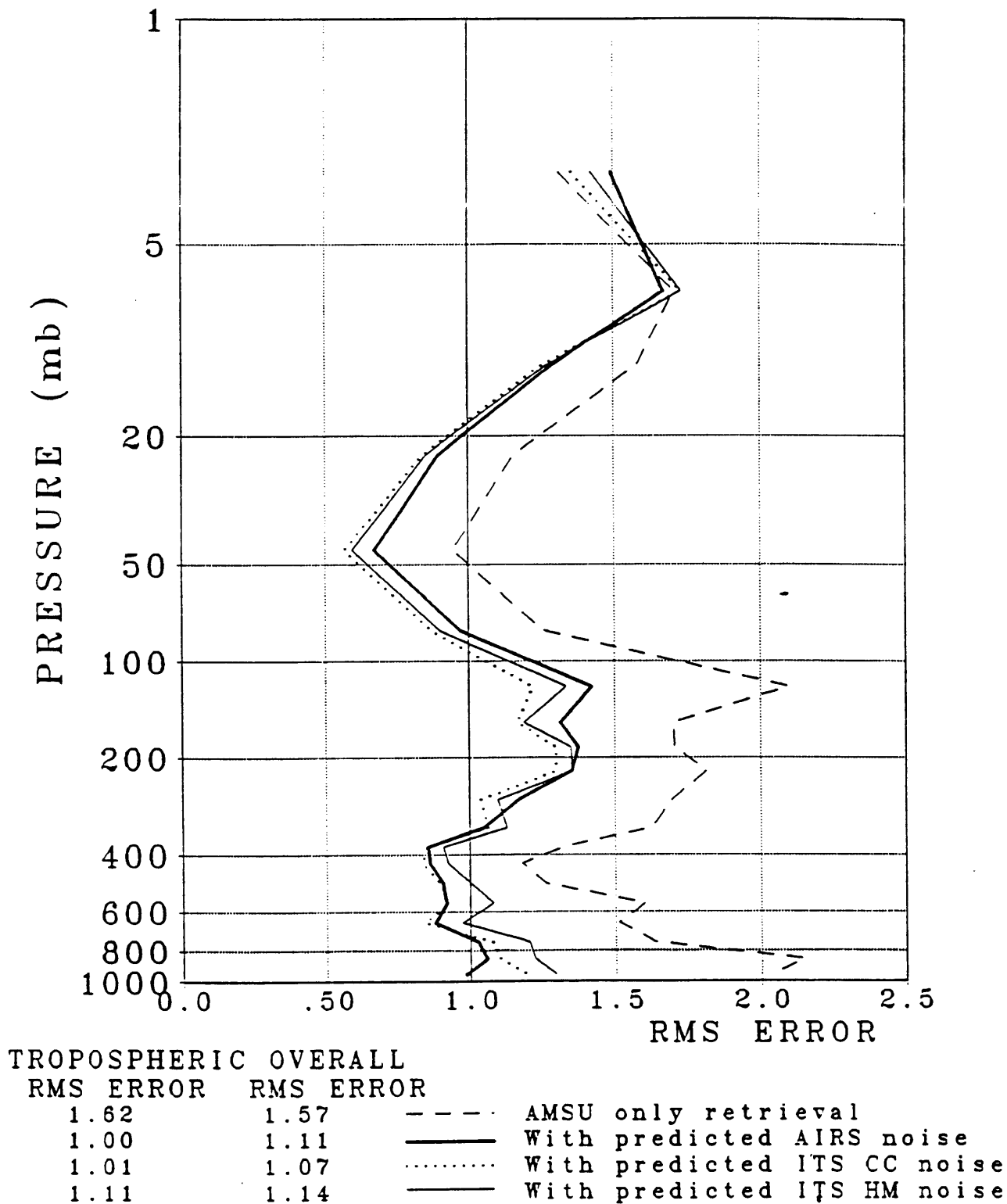


Figure 4

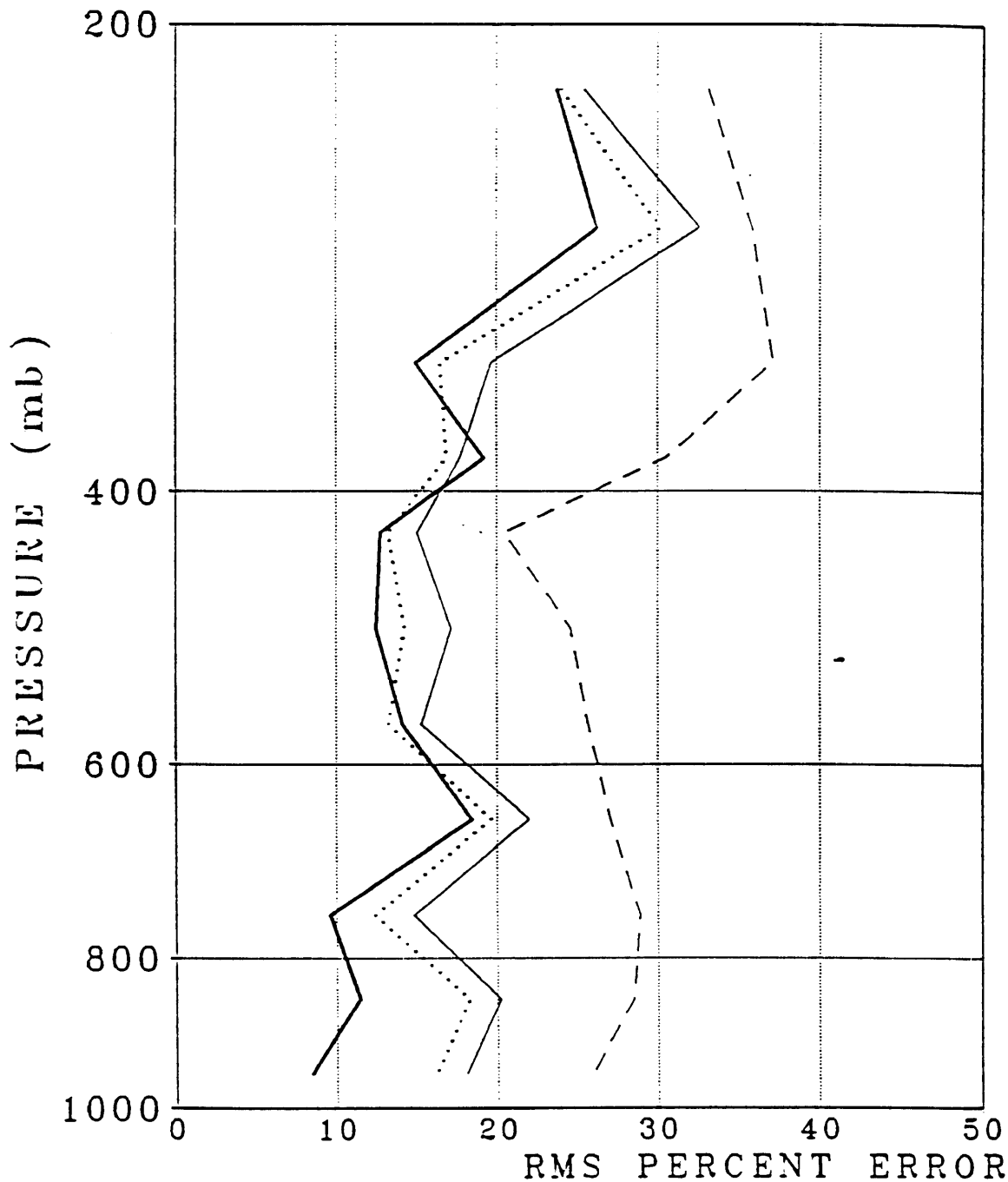
# Figure 5

AIRS/AMSU DAYTIME 300 mb 50% CLOUDY  
LAYER MEAN RMS TEMPERATURE ERRORS (°C)



# Figure 6

AIRS/AMSU DAYTIME 300 mb 50% CLOUDY  
1 Km LAYER PRECIPITABLE WATER PERCENT ERRORS



RMS ERROR OF TOTAL

%	gm/cm <sup>2</sup>
20.77	0.67
1.38	0.04
8.92	0.29
10.85	0.35

----	AMSU B only retrieval
————	With predicted AIRS noise
.....	With predicted ITS CC noise
————	With predicted ITS HM noise

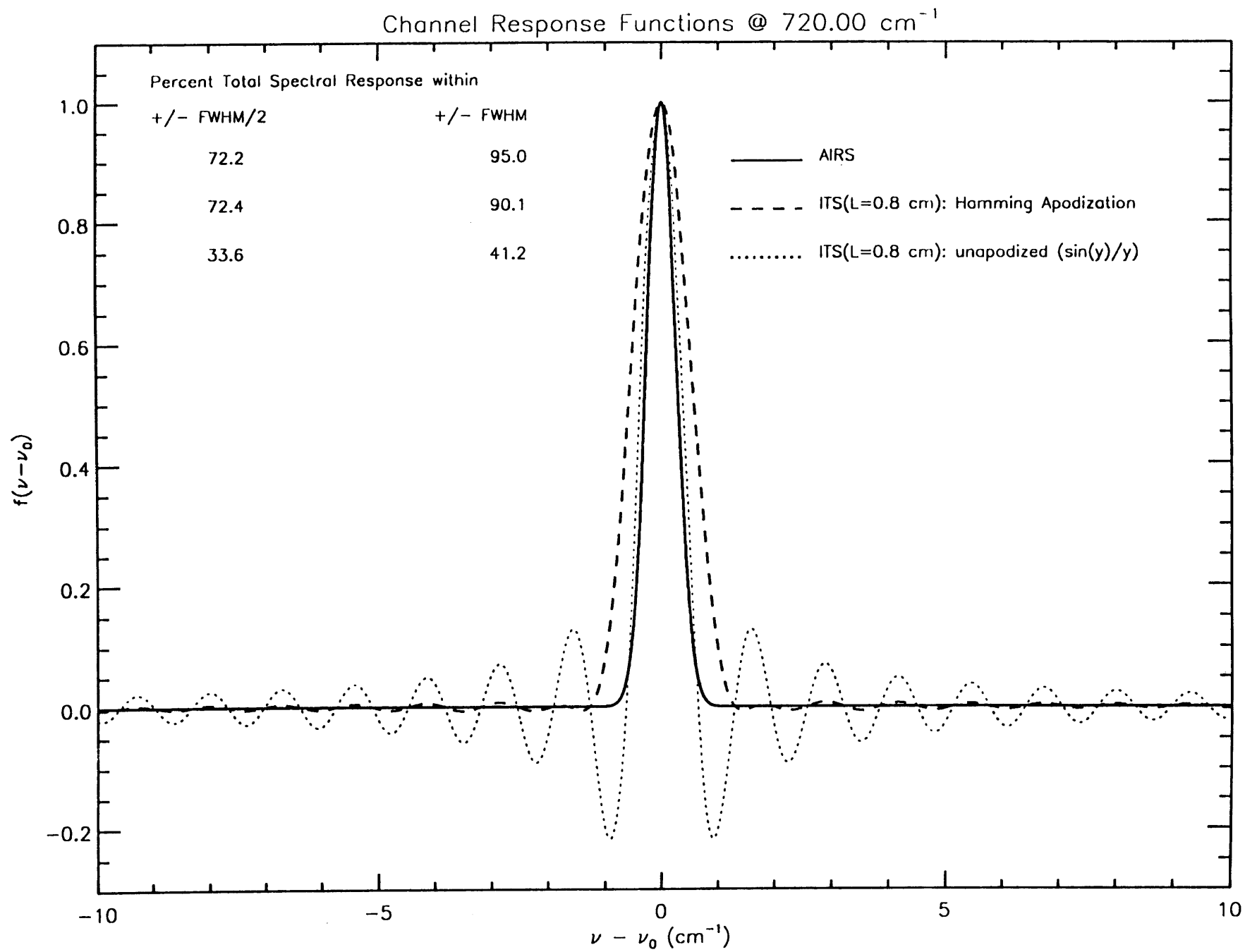
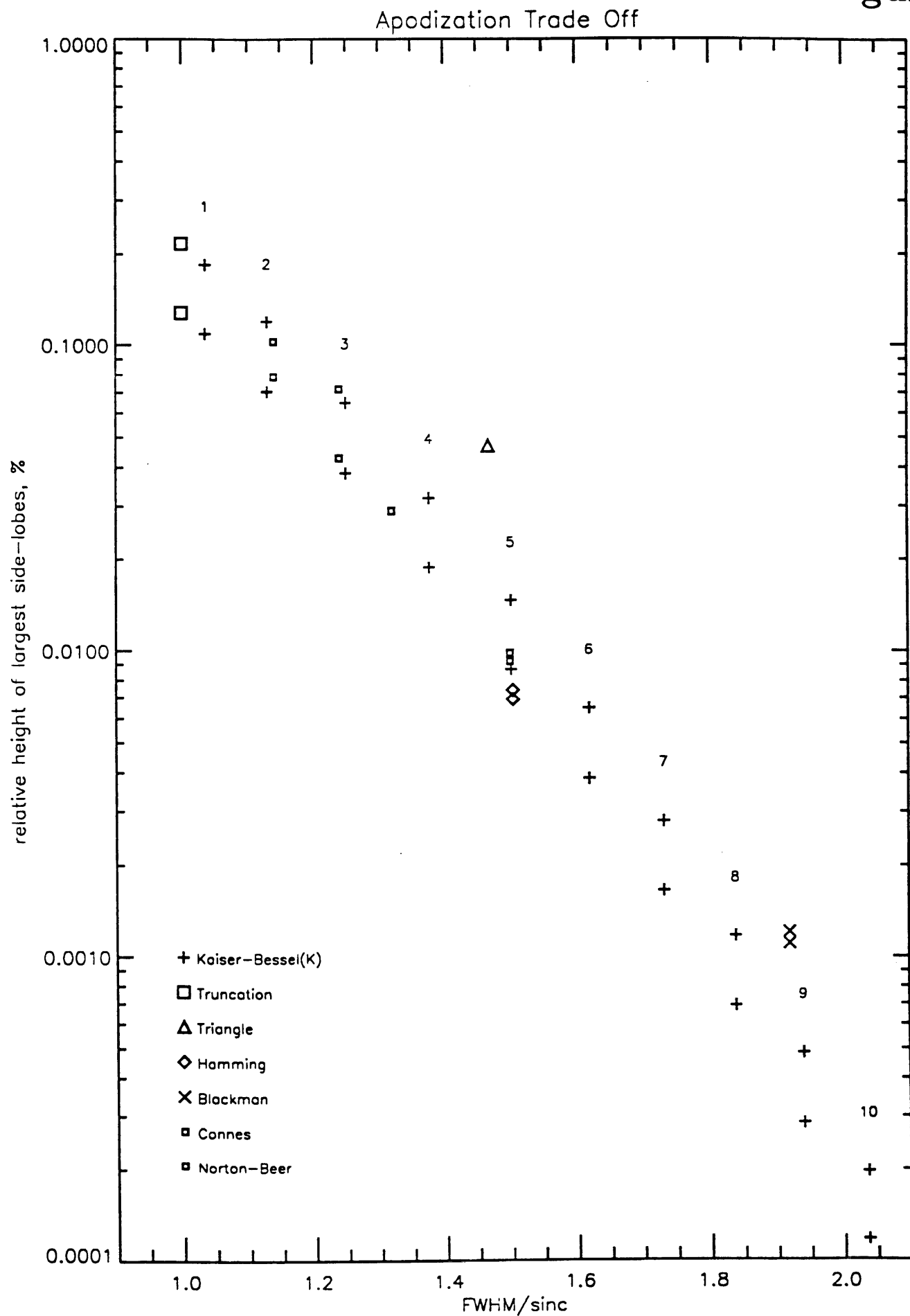
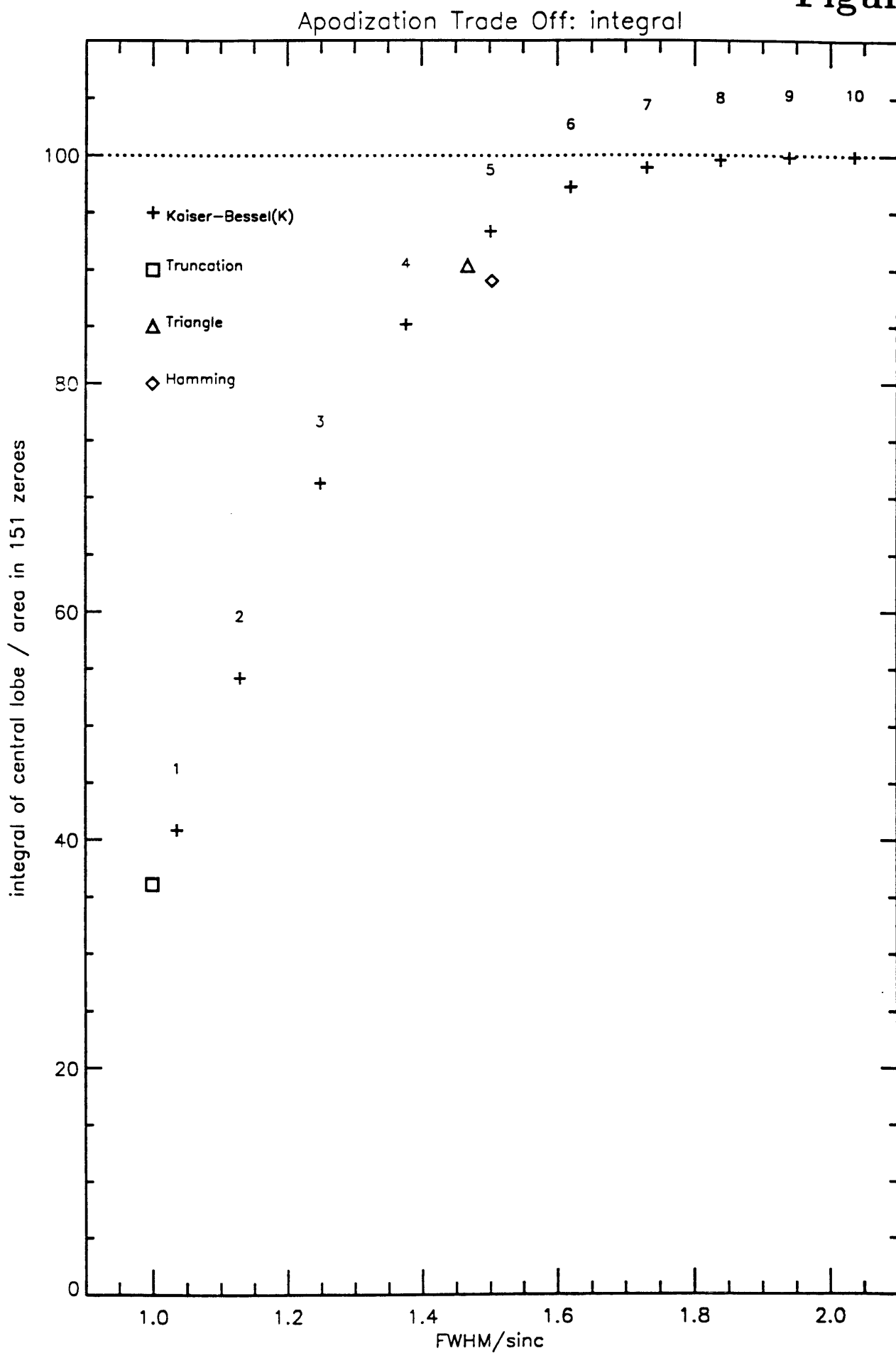


Figure 7

# Figure 8



# Figure 9



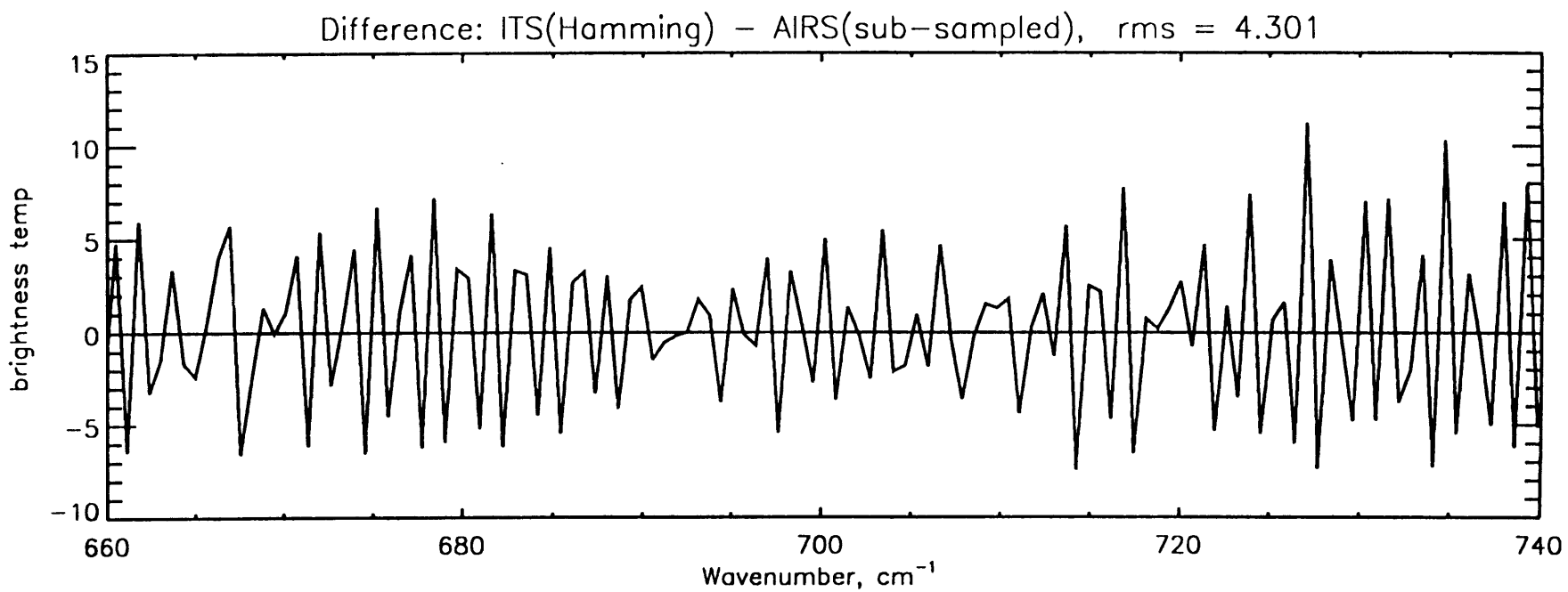
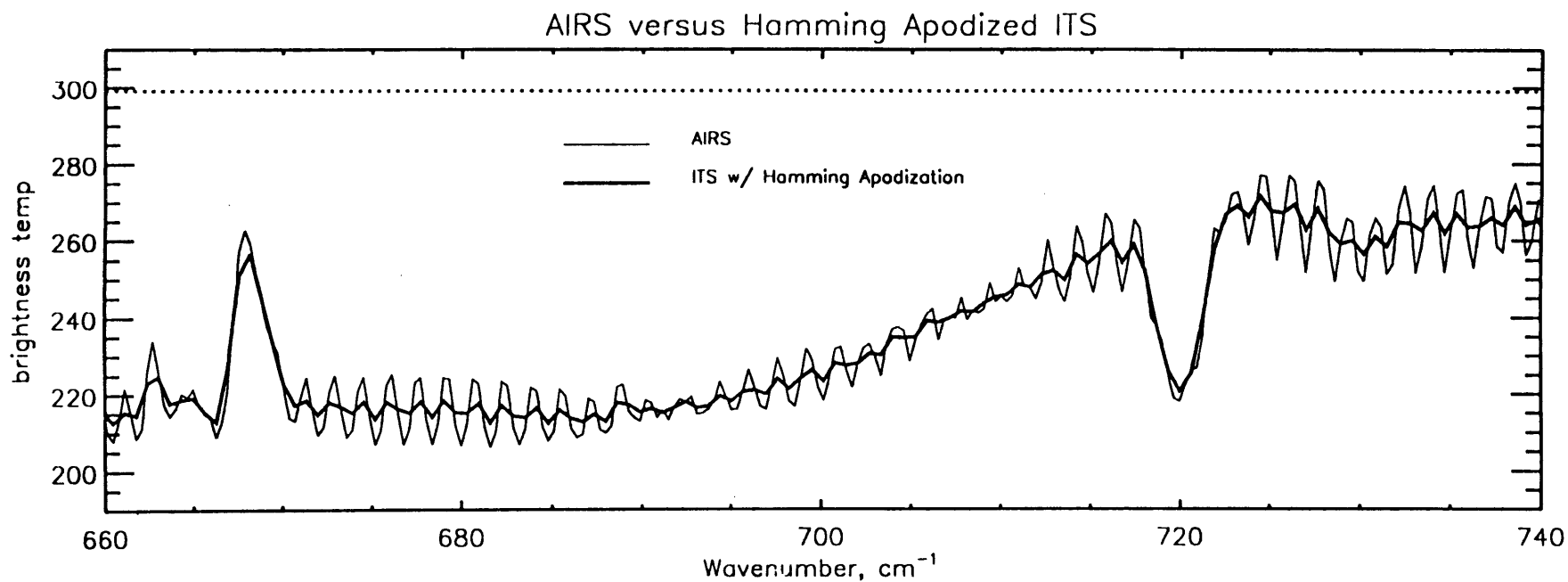


Figure 10

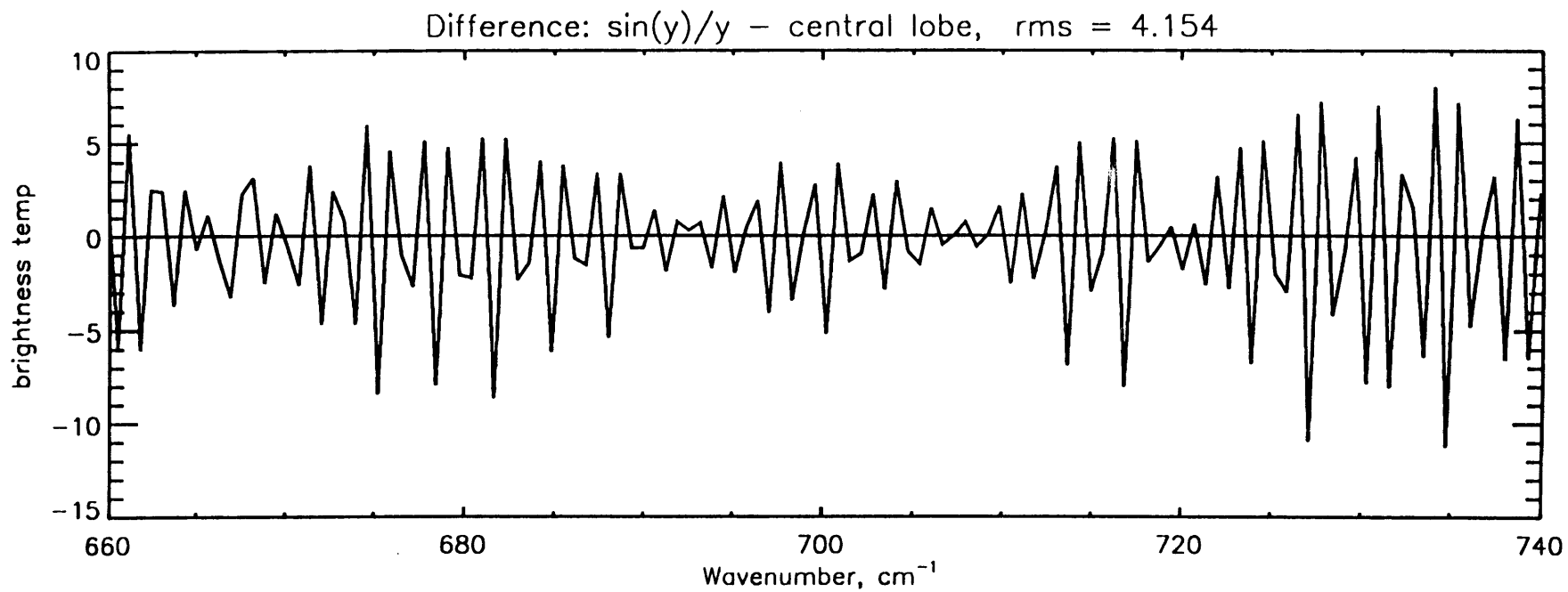
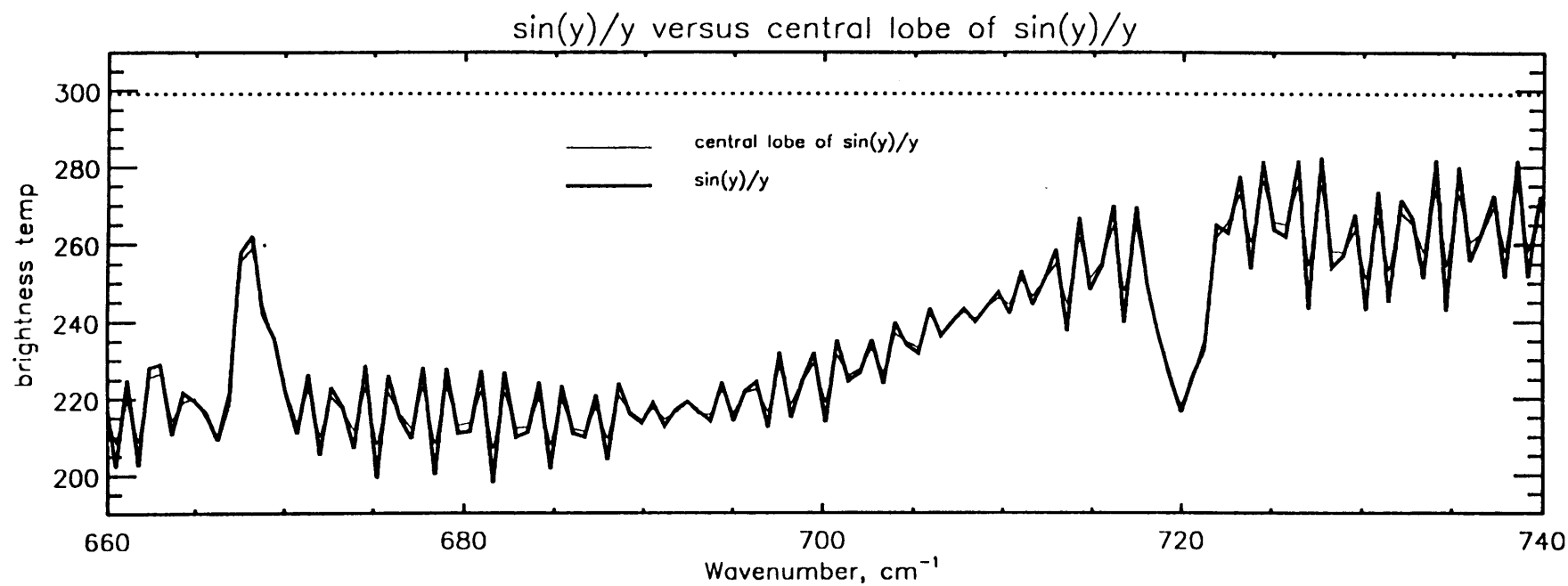
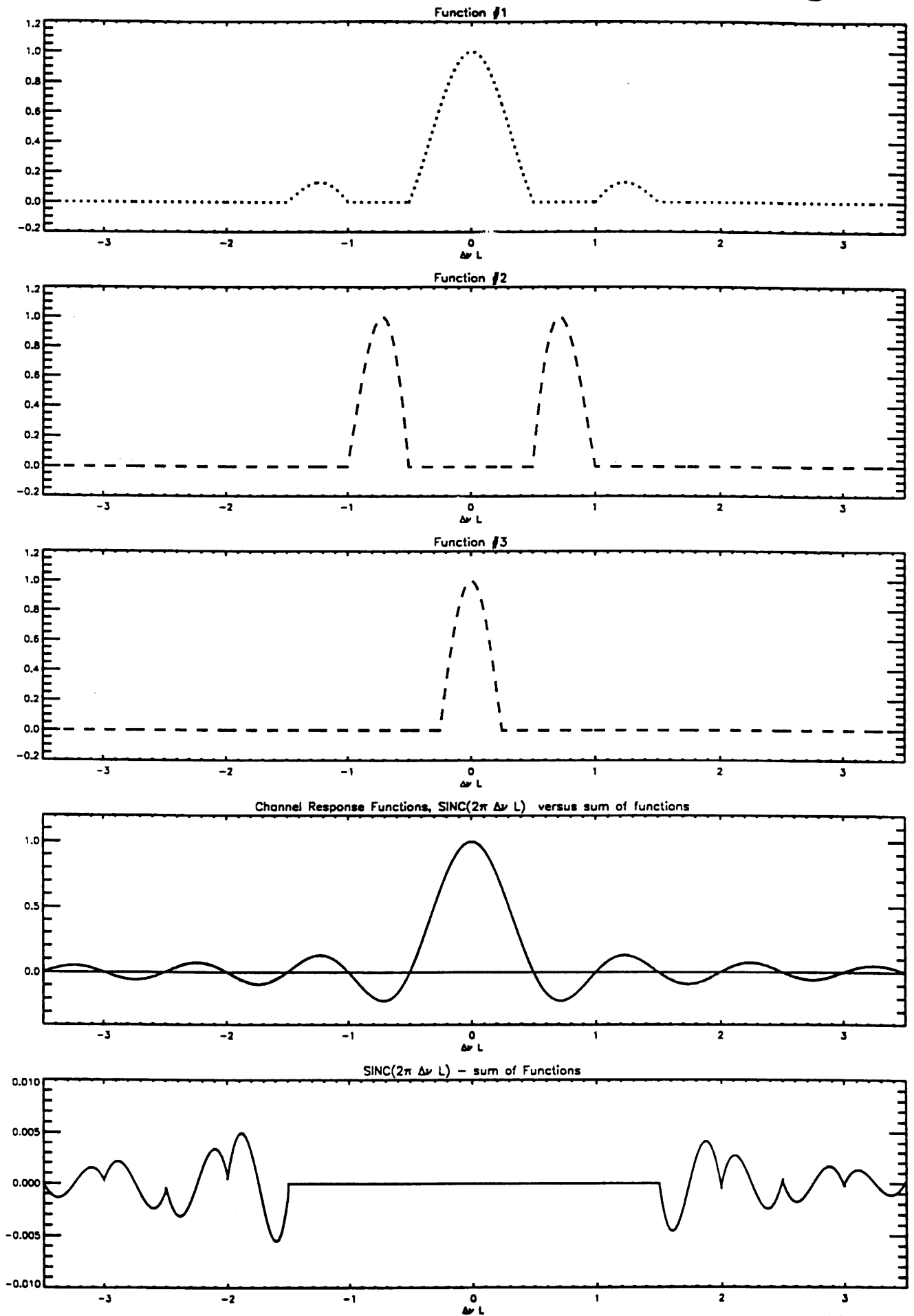


Figure 11

# Figure 12



35

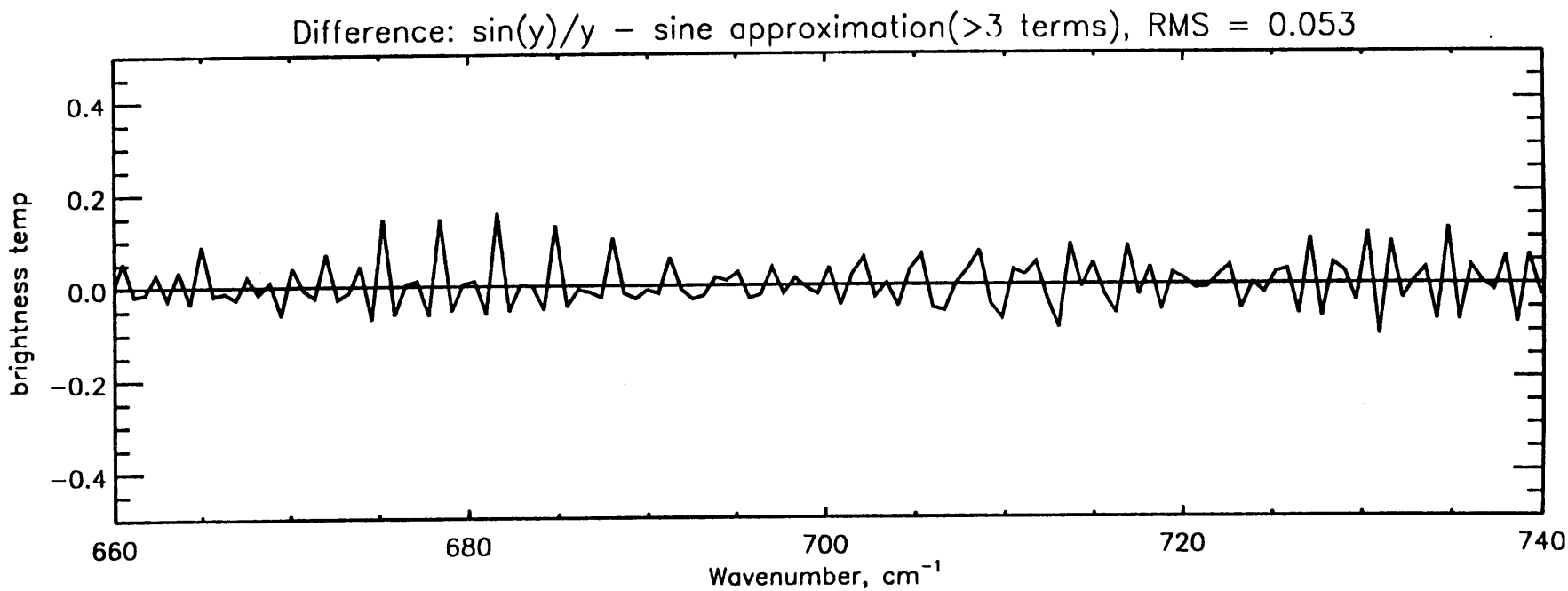
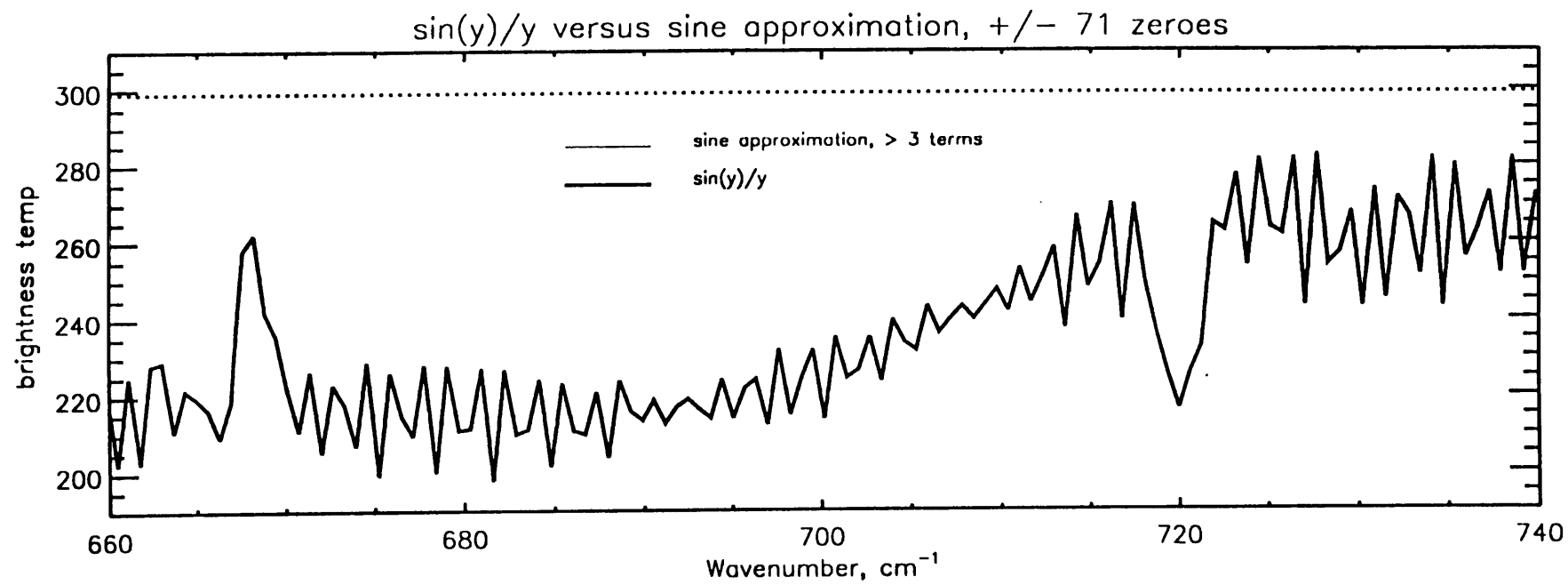


Figure 13